Exciton spectroscopy of optical reflection from wide quantum wells

E. S. Khramtsov, P. S. Grigoryev, D. K. Loginov, and I. V. Ignatiev
Spin Optics laboratory, St. Petersburg State University, Ulyanovskaya 1, Petrodvorets, 198504 St. Petersburg, Russia

Yu. P. Efimov, S. A. Eliseev, and P. Yu. Shapochkin
Department of Physics, St. Petersburg State University, Ulyanovskaya 1, Petrodvorets, 198504 St. Petersburg, Russia

E. L. Ivchenko
Ioffe Institute, Russian Academy of Sciences, 194021 St. Petersburg, Russia
and Department of Physics, St. Petersburg State University, Ulyanovskaya 1, Petrodvorets, 198504 St. Petersburg, Russia

M. Bayer
Experimentelle Physik 2, Technische Universität Dortmund, D-44221 Dortmund, Germany and Ioffe Physical-Technical Institute, Russian Academy of Sciences, 194021 St. Petersburg, Russia

(Received 24 October 2018; published 22 January 2019)

Optical spectroscopy of resonant reflection has been used for both experimental and theoretical studies of the exciton-light interaction in wide, high-quality quantum-well structures with the widths exceeding the exciton Bohr radius by an order of magnitude or more. The light mixes the low-lying confined exciton states which are captured by the generalized model developed by M. M. Voronov *et al.* [Phys. Solid State **49**, 1792 (2007)]. We demonstrate that the high-energy confined states in the wide QWs can still be described by the standard model in which the amplitude reflection coefficient from the QW is a sum of individual size-quantized exciton resonances. The excitonic parameters extracted from fitting the experimental spectrum to the standard model agree with those obtained by the numerical solution of the two-particle Schrödinger equation in a rectangular quantum well. The measured and microscopically calculated spectra are compared with those found with the widely used model of the center-of-mass exciton quantization and the polaritonic model. The comparison shows that the two approximate models considerably underestimate the interaction of confined excitons with light because they ignore the strong modification of the exciton wave function near the QW interfaces.

DOI: 10.1103/PhysRevB.99.035431

I. INTRODUCTION

In the excitonic spectroscopy of semiconductor heterostructures, the concepts of narrow and wide quantum wells (QWs) are tied to the ratio between the well thickness L and the bulk exciton Bohr radius a_B. In the narrow QWs, where the width L is of the order of or smaller than a_B, the exciton resonances are spectrally well separated by the single-particle quantum-confinement energies [1–11]. Each spectral resonance related to a particular quasi-two-dimensional exciton state can be readily described by the standard theory of exciton-light interaction. This theory involves three parameters, the exciton resonance frequency ω_0 and the radiative and nonradiative damping rates, Γ_0 and Γ, respectively [2,12]. It has been extended for wider QWs and applied for the description of the reflection spectra taken from QWs of thickness $L \sim 8a_B$ [13] with multiple, yet distinct, resonances due to excitons quantized as a whole particle. Any asymmetry of the QW potential can also be accounted for [14].

A further increase in the well width leads to a reduction of the energy spacing between the confined exciton levels and their stronger coupling through the electromagnetic wave. The standard theory of single-resonance optical reflection [2] was generalized in [15] to make allowance for the light-induced mixing of multiple excitonic states. In the present work we study the reflection spectra taken from submicron-thick layers with $L > 10a_B$ and analyze them in the frame of the single- and multiple-resonance theories. It is shown that the simple single-resonance description is valid as soon as the spectral separation between the nearby exciton states, $\omega_{0,j+1} - \omega_{0,j}$, exceeds the radiative damping rates $\Gamma_{0j}, \Gamma_{0,j+1}$ and the light-induced frequency renormalizations $\delta\omega_{0,j}, \delta\omega_{0,j+1}$. We demonstrate that these criteria may be fulfilled in very wide QW layers, but for excited confined-exciton states with large enough indices j. The great advantage of such an approach is that it allows one to extract from the experimental optical spectra the parameters $\tilde{\omega}_{0,j} = \omega_{0,j} + \delta\omega_{0,j}$, Γ_{0j}, and Γ_j without resorting to particular microscopic treatments [16] and polaritonic models. The latter include many assumptions concerning the spatial behavior of the exciton wave function near the interfaces, including additional boundary conditions, "no-escape" boundary conditions [17,18], and an additional surface layer free of excitons ("dead layer") [19–23]. The second aim of this work is verification, based on the extracted excitonic parameters, of the applicability of the center-of-mass (c.m.) and polaritonic models in thick-layer wells. We show that these models strongly underestimate the strength

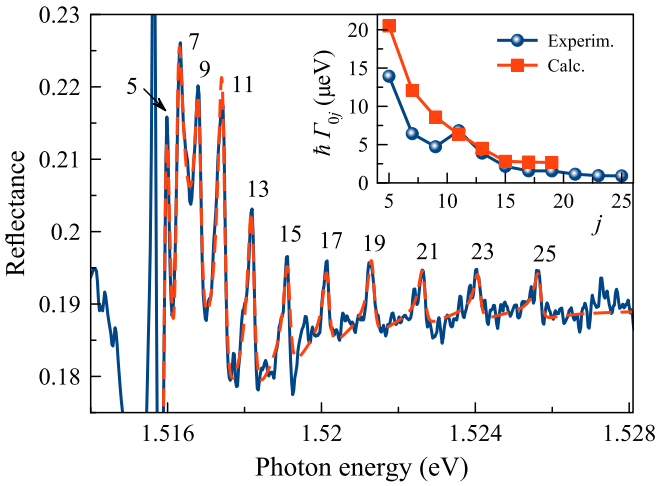

FIG. 1. Normal-incidence reflection spectrum of the 240-nm $GaAs/Al_{0.28}Ga_{0.72}As$ QW (blue curve) and the fit by Eqs. (1) and (2) (dashed red curve). Numbers indicate the exciton resonances corresponding to the quantization of exciton center-of-mass motion in this wide QW. The inset shows the radiative broadenings of different excitonic resonances, $\hbar\Gamma_{0j}$, extracted from the reflection spectrum (blue dots) and obtained in the microscopic modeling (red squares). Sample temperature $T = 1.5$ K.

of the exciton-light interaction for the high-energy confined exciton states.

II. FITTING OF EXPERIMENTAL SPECTRA TO THE STANDARD MODEL

Figure 1 shows the reflection spectrum of the structure containing a submicron GaAs/AlGaAs QW with width $L = 240$ nm grown between the $Al_{0.28}Ga_{0.72}As$ barriers; the thickness of the top barrier $L_b = 266$ nm. The denoted reflection peaks are attributed to optical transitions to the exciton states resulting from quantum confinement of the heavy-hole exciton as a whole. The light-hole exciton transitions are less efficient and more broadened and usually can be distinctly resolved only in the low-energy range of reflection spectra of wide QW structures [22]. Light-hole excitons reveal themselves in magnetic field when oscillator strength is increased [24]. They are merely observable in Fig. 1; therefore, we leave them out of the consideration in the experimental data analysis.

To quantitatively describe the exciton-light interaction, we use the phenomenological model for reflection spectra outlined in Ref. [12] and generalized in Refs. [13,14] for the case of multiple exciton transitions. Hereafter, we refer to it as to the standard model. Its applicability to the wide QWs will be clarified in Sec. III. The optical reflection from the heterostructure is then described by

$$R = \left|\frac{r_s + r_{QW}}{1 + r_s r_{QW}}\right|^2, \quad r_{QW} = e^{2i\phi}\sum_j e^{2i\psi_j} r_j. \qquad (1)$$

Here the index j enumerates the exciton resonances, r_s is the amplitude reflection coefficient from the sample surface ($r_s < 0$), and ϕ is the phase shift of the light wave over the distance $L_b + (L/2)$. The contribution r_j of the jth resonance to the total amplitude reflection coefficient from the QW layer is given by [2,12]

$$r_j = \frac{i\Gamma_{0j}}{\tilde{\omega}_{0,j} - \omega - i(\Gamma_j + \Gamma_{0j})}, \qquad (2)$$

with the j-exciton parameters $\tilde{\omega}_{0,j}$, Γ_{0j}, and Γ_j being defined in the Introduction and considered fitting parameters for each exciton resonance. Finally, ψ_j is an additional phase shift determined by the spatial variation $\Phi(z) \equiv \varphi(z, z, 0)$ of the exciton envelope wave function $\varphi(z_e, z_h, |\boldsymbol{\rho}_e - \boldsymbol{\rho}_h|)$ taken at the coinciding electron and hole coordinates [14]

$$\tan\psi_j = \frac{\int \Phi(z)\sin(qz)dz}{\int \Phi(z)\cos(qz)dz}. \qquad (3)$$

Here $q = n_b\omega/c$ is the light wave number with the refractive index $n_b = 3.6$ of the barrier material assumed to coincide with the background refractive index of the QW material n_{QW}. For a symmetric QW potential, the values of the phase factor $\exp(2i\psi_j)$ for even and odd exciton envelopes reduce to 1 and -1, respectively. An asymmetry of the QW profile leads to a deviating phase difference, $\psi_j - \psi_{j+1} \neq \pm\pi/2$ [14]. Thus, for the asymmetric QWs the exciton resonance is characterized by the fourth fitting parameter ψ_j.

The generalization of Eqs. (1) and (2) with an allowance for the refractive index mismatch, $n_b \neq n_{QW}$, is given in Ref. [25]. For the GaAs/AlGaAs and InGaAs/GaAs heteropairs with low content of aluminum or indium, the mismatch is negligible. However, due to this mismatch, an additional reflection occurs at the QW interfaces. In addition, there is a smooth increase in the refractive index n_{QW} in the spectral range under consideration. We treat these weak effects as giving rise to a smoothly varying additive correction δR_b to the reflection coefficient (1) which can be approximated by the empirical function

$$\delta R_b = R_b\{1 - \exp[-(E - E_0)/\delta E]\},$$

with $R_b = 0.038$, $E_0 = 1.516$ eV, and $\delta E = 2.1$ meV.

As seen from Fig. 1, starting from the index $j = 5$ the excited-exciton resonances are perfectly described by Eqs. (1) and (2) of the standard model. Only the odd resonances are fitted because these features are clearly distinguishable. For the spectrum in Fig. 1 the manifestation of excitons with even j is suppressed [see the comment following Eq. (17) in Sec. IV]. Briefly, the suppression of even or odd states is related to the ratio of the QW width to the light wavelength.

The inset in Fig. 1 shows the exciton radiative broadening $\hbar\Gamma_{0j}$ obtained from the fitting. In order to minimize the number of fitting parameters, we took the same values of the nonradiative broadening, $\hbar\Gamma_j = 100\,\mu$eV, and the phase, $2(\phi + \psi_j) = 3.8$, for the resonances with $j \geqslant 7$. As seen from the inset, the exciton-light interaction described by Γ_{0j} gradually diminishes with increasing the state index from $j = 5$. Such behavior is described in modeling terms in the next section.

III. ALLOWANCE FOR LIGHT-INDUCED MIXING OF MULTIPLE EXCITONIC STATES

In this section we check the validity of the calculation procedure based on Eqs. (1) and (2), turning to the theory [15] and

making allowance for the light-induced mixing of excitonic levels $\tilde{\omega}_{0,j}$.

The mechanical (or bare) exciton wave functions $\psi_j(z_e, z_h, \rho)$ and energies $\hbar\omega_{0,j}$ of several confined states are calculated by direct numerical solution of the three-dimensional Schrödinger equation for an exciton in a QW. Here $\rho = |\boldsymbol{\rho}_e - \boldsymbol{\rho}_h|$ is the relative electron-hole distance in the interface plane. The method is described in Refs. [26,27]. Only the s-like exciton ground state of the relative electron-hole motion is taken into account. The higher s states of the relative motion make almost no contribution to the reflection spectra. The calculation is performed for heterostructures with rectangular GaAs/$Al_{0.3}Ga_{0.7}As$ QWs. The material parameters of this heterostructure are the same as used in Ref. [26]. For simplicity, the complicated band structure of the valence band is ignored, and the light-hole exciton states are not included in the consideration.

The exciton radiative damping may be thought of as a measure of the exciton-light interaction or the oscillator strength of the transition from the ground (vacuum) to exciton state. It is calculated from [12,26]

$$\Gamma_{0j} = \tfrac{1}{2} q\omega_{LT}\pi a_B^3 |f_j|^2, \tag{4}$$

where

$$f_j = \int \Phi_j(z) \mathrm{e}^{\mathrm{i}qz} dz, \tag{5}$$

ω_{LT} is the longitudinal-transverse splitting in frequency units, and a_B is the bulk exciton Bohr radius.

First, we analyze the dependencies of the exciton radiative decay Γ_{0j} and spectral shift $\delta\omega_{0,j}$ on the QW width. The results of the calculation are presented in energy units in Fig. 2. As seen from Fig. 2(a), the lowest exciton transition is most intensive for QWs with L below 150 nm, in agreement with numerous experiments. With increasing the QW width, the intensity of the second transition rises and saturates at $L = 250$ nm; then it decreases and, at $L \approx 290$ nm, falls below the increasing intensity of the transition $j = 3$. Other transitions are less efficient in the studied range of L. The critical values of the QW width, 150 and 290 nm, slightly exceed the half and full wavelengths, $\lambda/2$ and λ, of the light wave inside the medium.

The light-induced spectral shift of the exciton states is calculated as [12]

$$\delta\omega_{0,j} = \frac{1}{2} q\omega_{LT}\pi a_B^3 \times \iint \Phi_j(z)\Phi_j(z') \sin(q|z - z'|) dz dz'. \tag{6}$$

It follows from Fig. 2(b) that the energy shift $\hbar\delta\omega_{0,1}$ of the first exciton state increases with L, exceeds the value of 100 μeV in QWs with $L > 200$ nm, and reaches a smooth maximum at $L = 250$ nm, overcoming the energy gap between the first and second bare-exciton levels. For the excited levels, $j > 1$, the sign of the shift (6) may change with varying the QW width.

The calculated values of $\hbar\Gamma_{0j}$ and $\tilde{\omega}_{0,j}$ were used to simulate the reflection coefficient r_{QW} defined by Eq. (1) in the range $L = 100$–300 nm. Here, for the convenience of analysis, we assume an achromatic antireflection coating of the sample by setting $r_s = 0$ in Eq. (1). In this case all the exciton resonances appear in the reflection spectra as peaks. An exactly symmetric rectangular potential profile of the QWs is assumed so that the phases $2\psi_j$ in Eq. (1) are simply $j\pi$ [14]. The results of the calculations are shown in Fig. 3 by blue curves. In the modeling we introduce some small nonradiative broadening, $\hbar\Gamma_j = 5\,\mu$eV, which is the same for all exciton resonances. Typically, this parameter is an order of magnitude larger. We underestimate it here for better figure clarity. This broadening is a signature of exciton-phonon interaction; we addressed this matter in detail in another study [28].

To question the accuracy of the model (1) and (2) and clarify the role of the light-induced coupling of exciton states, we compare the spectra of the standard model with those obtained in the generalized theory of Voronov *et al.* [15]. They took the coupling into account and derived the following formula for the reflection coefficient r_{QW} from the quantum well:

$$r_{QW} = \frac{i}{2} e^{2i\phi} q\omega_{LT}\pi a_B^3 \sum_{jj'} M^{-1}_{jj'} f_j f_{j'}. \tag{7}$$

Here the indices j, j' run over the exciton manifold, and the multiresonance matrix $M_{jj'}$ is defined as follows

$$\hat{M} = \begin{pmatrix} \omega_{0,1} - \omega - \Omega_{11} - \mathrm{i}\Gamma_1 & -\Omega_{12} & -\Omega_{13} & \dots \\ -\Omega_{21} & \omega_{0,2} - \omega - \Omega_{22} - \mathrm{i}\Gamma_2 & -\Omega_{23} & \dots \\ -\Omega_{31} & -\Omega_{32} & \omega_{0,3} - \omega - \Omega_{33} - \mathrm{i}\Gamma_3 & \dots \\ \dots & \dots & \dots & \dots \end{pmatrix}, \tag{8}$$

with the coupling matrix elements being

$$\Omega_{jj'} = \Omega_{j'j} = \frac{i}{2} q\omega_{LT}\pi a_B^3 \times \iint \Phi_j(z)\Phi_{j'}(z') e^{iq|z-z'|} dz dz'. \tag{9}$$

Neglecting the off-diagonal elements $\Omega_{jj'}$ and replacing the diagonal elements by

$$\Omega_{jj} = -\delta\omega_{0,j} + i\Gamma_{0j},$$

we immediately obtain the coefficient r_{QW} of the standard model.

The spectra calculated from Eq. (7) are shown in Fig. 3 by red curves. As seen from Fig. 3, for the 100- and 150-nm QWs, the blue and red lines coincide, and one can see only the red color. The radiative energy shift of exciton state 1 is comparable to the energy gap $\hbar(\omega_{0,2} - \omega_{0,1})$ in the 150-nm QW. The individual spectral lines of the ground and first excited exciton states in this QW [dashed curves in Fig. 3(b)] overlap strongly, and the resulting contour looks like a single

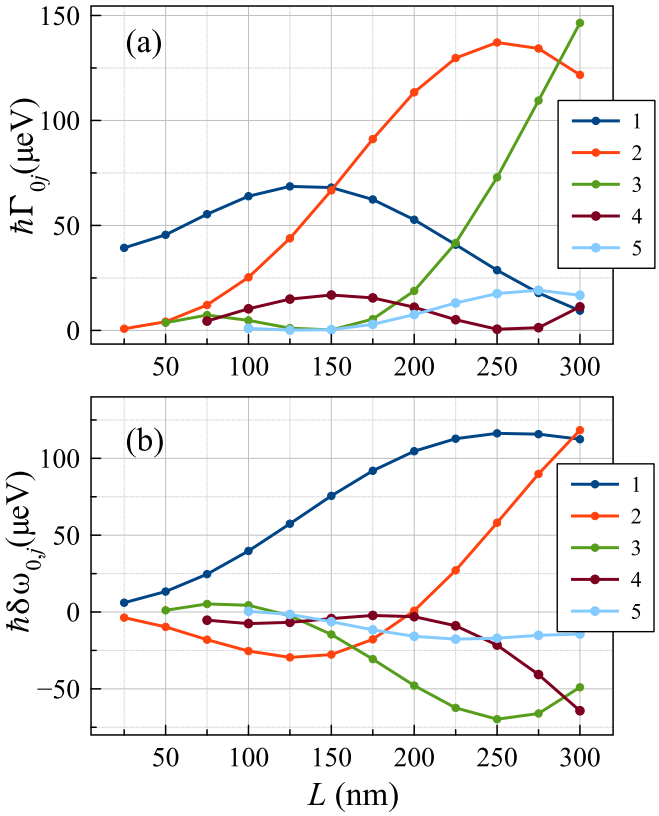

FIG. 2. QW-width dependencies of (a) the exciton radiative decay rates $\hbar\Gamma_{0j}$ and (b) the energy shifts $\hbar\delta\omega_{0,j}$ for several of the lowest exciton transitions in GaAs/$Al_{0.3}Ga_{0.7}$As QWs computed in the microscopic model.

peak in both models. Due to the difference in phases ψ_1 and ψ_2 by $\pi/2$, the resulting contour has a smaller area than the sum of the two separate contours.

For the wider QWs, $L = 200$ and 250 nm, the low-energy exciton states are strongly mixed by the exciton-light interaction, and the difference between the two models is remarkable in this spectral region. In particular, the light-induced mixing strongly modifies the reflectance of the first two states in the 200-nm QW and the first five states in the 250-nm QW. In both cases, the overall reflection in the strong-coupling region is significantly smaller than the sum of individual exciton contributions $|r_j|^2$. This occurs because of the destructive interference of the exciton transitions.

The blue and red high-energy parts of the spectra, $j \geqslant 4$ for the 200-nm QW and $j \geqslant 6$ for the 250-nm QW, coincide with one another in detail. Therefore, in this range the standard model can surely be applied to the analysis of the measured reflection spectra.

In order to quantitatively visualize the accuracy of the standard model, we have calculated reflection spectra using the generalized model (8) with a modified coupling matrix $\hat{M}$. Namely, we have set one of the off-diagonal elements $\Omega_{jj'}$ to zero and calculated the relative integral difference of the spectra. The results for the modulus of the difference are shown in Fig. 4. As seen, the difference is within 2% for the 100-nm QW if $\Omega_{13} = \Omega_{31}$ is nullified. It is considerably larger and reaches tens of percent for the 200-nm QW if we nullify $\Omega_{13} = \Omega_{31}$ or $\Omega_{24} = \Omega_{42}$. This means that the light-induced coupling of the first four states is significant in this QW. In the case of the 300-nm QW, the first five states are strongly coupled.

IV. EXCITON-LIGHT INTERACTION IN THE CENTER-OF-MASS QUANTIZATION MODEL

Here we compare the exciton-light interaction strengths of the excited confined exciton states obtained by numerical solution of the Schrödinger equation with the results of the conventional c.m. model.

In Fig. 5(a), dots show the exactly calculated function $\Phi_j(z)$ of the exciton confined state $j = 9$ in the 240-nm GaAs/AlGaAs QW, while the solid curve represents the best fitting by the c.m. quantization model [12]. In this widely used model, the internal electron-hole motion and exciton motion as a whole are considered independently of each other, and the exciton wave function at the coinciding coordinates, $\boldsymbol{r}_e = \boldsymbol{r}_h$, is written as

$$\Phi_j^{\text{c.m.}}(z) = \sqrt{\frac{2}{\pi a_B^3 L}} \begin{cases} \cos(K_j z) & \text{for odd } j, \\ \sin(K_j z) & \text{for even } j, \end{cases} \tag{10}$$

where $K_j = \pi j/L$. The left- and rightmost zeros of $\Phi_9(z)$ are shifted from the interfaces by some distance L_9^d, the transition layer (or dead layer) width. It follows then that, while comparing $\Phi_j^{\text{c.m.}}(z)$ with the exact function $\Phi_j(z) = \varphi_j(z, z, 0)$, the well width in Eq. (10) should be replaced by $L_j^\star = L - 2L_j^d$, which gives for the exciton kinetic energy [13]

$$\varepsilon_j = \frac{\hbar^2}{2M}\left(\frac{\pi}{L_j^\star}\right)^2, \tag{11}$$

where M is the exciton translational effective mass.

The fitting in Fig. 5(a) is very good in the bulk region but reveals a significant discrepancy in the regions neighboring the boundaries. As shown below, this interface-induced difference strongly affects the radiative exciton decay rate.

There is a temptation to improve the c.m. model taking into account the interface-induced distortion of the effective lateral Bohr radius as follows:

$$\varphi_j(z, z, \rho) = \varphi_j(z, z, 0)\mathrm{e}^{-\rho/a_B(z)}, \tag{12}$$

where $\varphi_j(z, z, 0)$ is the exact solution at $\boldsymbol{r}_e = \boldsymbol{r}_h$. Figure 5(b) shows the z dependence of the best-fit parameter $a_B(z)$. It is constant in the bulk but reveals a peculiar behavior near the zeros of $\varphi_j(z, z, 0)$. In addition to the fitting parameter $a_B(z)$ characterizing the ρ dependence of $\varphi_j(z, z, \rho)$ at a given z in the full region of ρ we introduce another lateral length,

$$a_0(z) = -\frac{\varphi(z, z, 0)}{[\partial\varphi(z, z, \rho)/\partial\rho]_{\rho=0}}, \tag{13}$$

which characterizes the local ρ dependence near $\rho = 0$. Figure 5(c) represents the function $a_0(z)$, which also demonstrates the specific behavior near the zeros of $\varphi_j(z, z, 0)$.

In order to explain such behavior of $a_B(z)$ and $a_0(z)$, let us expand $\varphi_j(z, z, \rho)$ near one of the zeros z_s in powers of $(z - z_s)$ and ρ as follows:

$$\varphi(z, z, \rho) \approx \partial_z\varphi\,(z - z_s) + \rho[\partial_\rho\varphi + \partial_{z\rho}\varphi\,(z - z_s)], \tag{14}$$

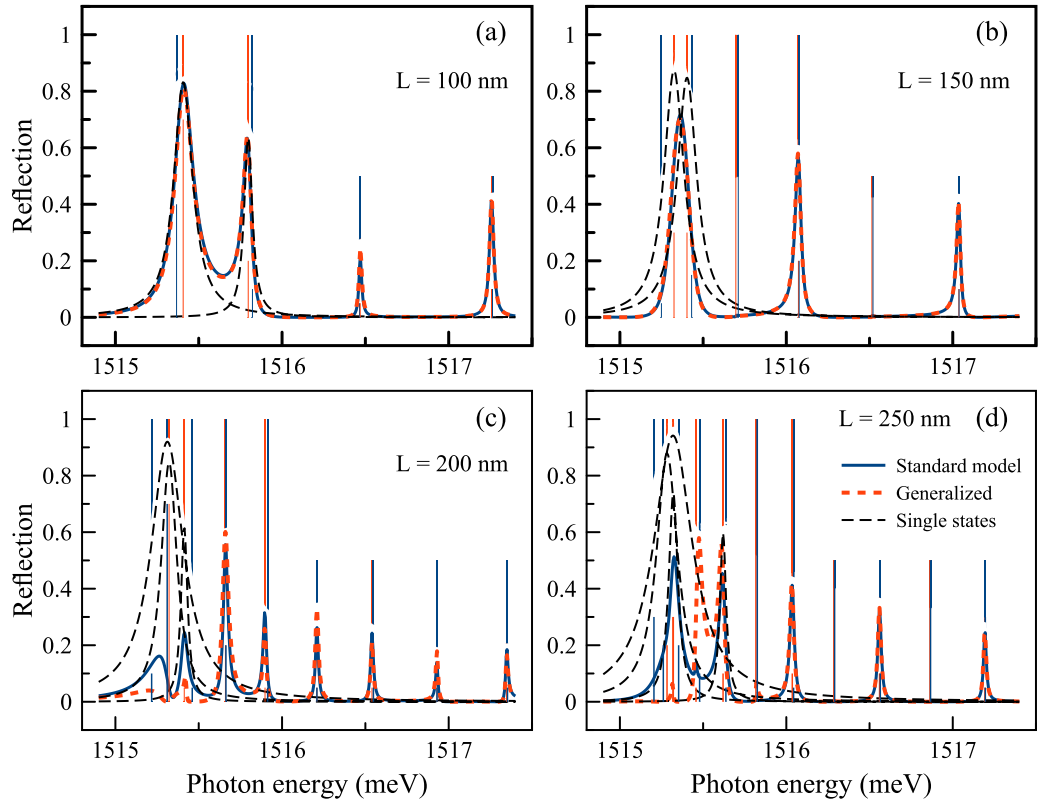

FIG. 3. Theoretically modeled reflection spectra of heterostructures with rectangular GaAs QWs with width $L = 100$, 150, 200, and 250 nm. The spectra are calculated using the standard model, Eqs. (1)–(6) (blue curves), and the generalized model, Eq. (7) (red curves). In (a) and (b) the blue and red curves coincide. Dashed curves calculated as $R_j = |r_j|^2$ show the artificially separated exciton resonances $j = 1$ and $j = 2$ in the low-energy spectral region. Vertical lines indicate the energy positions of the bare exciton states (blue lines) and their radiative shift (red lines).

where the partial derivatives, i.e., the second derivative $\partial_{z\rho}\varphi = \partial^2\varphi/\partial z\partial\rho$, are taken at $z = z_s$, $\rho = 0$. For zeros z_s in the layer middle, the relative and c.m. motions are uncoupled, and $\varphi'_\rho = 0$. At the outermost zeros where the interface effect is essential, the value of φ'_ρ differs from zero, but the second derivative should be retained anyway. In accordance with the presentation (12) we take $\varphi_j(z, z, 0) = \varphi'_z(z - z_s)$ as a common factor and obtain

$$\varphi(z, z, \rho) = \partial_z\varphi\,(z - z_s)\left(1 - \frac{\rho}{a_0(z)}\right), \qquad (15)$$

where

$$a_0(z) = \frac{\bar{a}}{1 - \frac{\ell}{z - z_s}}, \quad \bar{a} = \frac{\partial_z\varphi}{\partial_{z\rho}\varphi}, \quad \ell = \frac{\partial_\rho\varphi}{\partial_z\varphi}\bar{a}. \qquad (16)$$

The red curves in Fig. 5(c) are calculated from (16) using the best-fit parameters $\bar{a} = 14.5$ nm, $\ell = 2.2 \times 10^{-4}$ nm for $z_s = 61$ nm and $\bar{a} = 14.5$ nm, $\ell = -2.2 \times 10^{-3}$ nm for $z_s = 85$ nm.

In the framework of the c.m. model, the radiative decay rate is calculated by the replacement of L by $L^\star_j$ in the functions (10) and substituting them into Eqs. (4) and (5). The integration over z yields

$$\Gamma^{\text{c.m.}}_{0j} = \frac{2\pi^2 j^2 q L^\star \omega_{LT}}{\left[(\pi j)^2 - \left(qL^\star_j\right)^2\right]^2}(1 \pm \cos qL^\star_j), \qquad (17)$$

where the plus and minus signs correspond to states with odd and even j, respectively. The effective width $L^\star_j$ is dependent on the exciton level number. For the 240-nm QW under study, this dependence can be approximated as $L^\star(j) = L^\star_0 + bj + aj^2$ with the three parameters $L^\star_0 = 208$ nm, $b = 2.00$ nm, $a = -0.036$ nm obtained from the fitting of the central part of the numerically computed functions $\Phi_j(z)$ with the c.m. functions (10). The ratio between damping rates for states with even j and odd $j + 1$ is proportional to

$$\frac{\sin^2(qL^\star_j/2)}{\cos^2(qL^\star_{j+1}/2)}.$$

For the studied sample with the 240-nm QW, this ratio is a few percent in the exciton frequency region. This explains the low oscillator strength of the excitons with even j in the experimental spectrum of Fig. 1.

The calculation shows that, for the few lowest confined exciton states, the functions $\Phi_j(z)$ found microscopically and those applied in the c.m. model lead to very close values of the radiative damping rate. However, as one can see from Figs. 6(b) and 6(c), with increasing the number j the relative deviation between the values of Γ_{0j} and $\Gamma^{\text{c.m.}}_{0j}$ becomes more and more noticeable. To understand the origin of this result we analyze in Fig. 6(a) the integrand product $\Phi_9(z)\exp(iqz)$ entering Eq. (5). Figure 6(a) shows this product for the ninth exciton state in the 240-nm QW. Due to the even symmetry

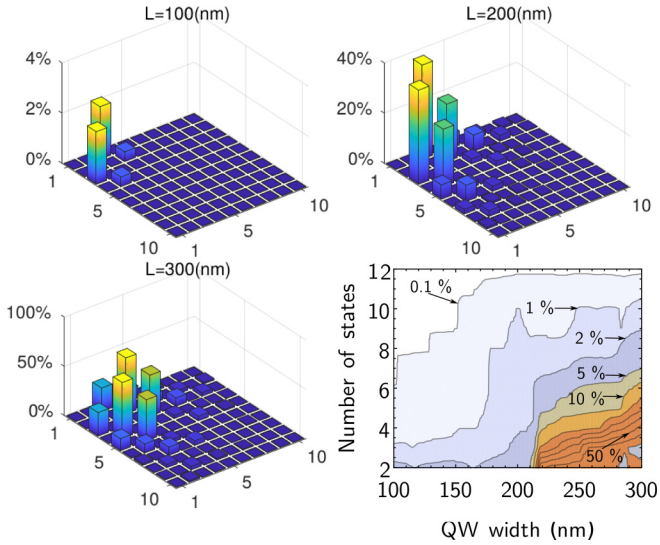

FIG. 4. Normalized integral difference of the spectra calculated using the total matrix M in Eq. (8) and the modified matrix with a pair of off-diagonal matrix elements $\Omega_{jj'} = \Omega_{j'j}$ set to zero. The horizontal axes indicate j and j'; the vertical axis is the normalized difference in percent. The bottom right panel shows the error estimate as a function of the number of coupled states and QW width.

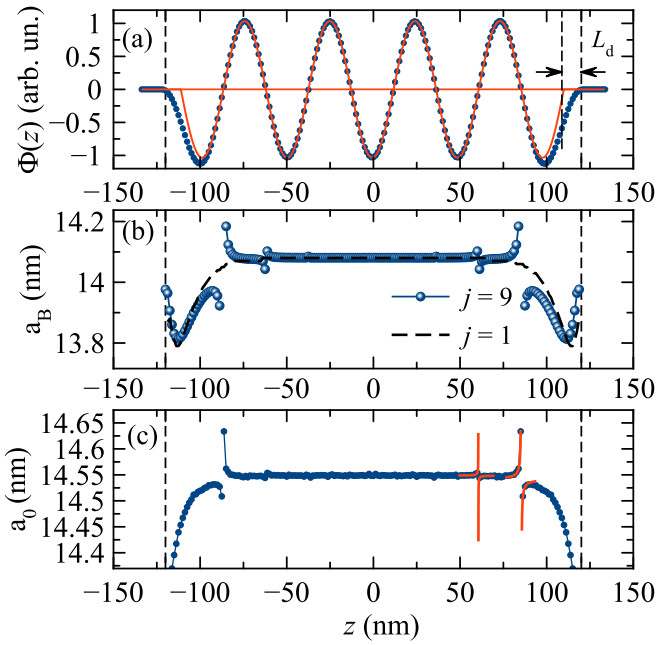

FIG. 5. (a) Cross section of the numerically obtained wave function for the ninth exciton state, $\Phi_9(z) = \varphi_9(z, z, 0)$, in the 240-nm GaAs/AlGaAs QW (dots). The cosine function (red line) is the best-fit wave function $\Phi_9^{\text{c.m.}}(z)$ of the c.m. model. Arrows marked by L_d show the transition layer. (b) The in-plane effective exciton Bohr radius introduced in Eq. (12) as a function of coordinate $z = z_e = z_h$ for the ninth state (dots) and the first state (black dashed line) of the exciton in the QW. (c) The local in-plane characteristic length a_0 defined by Eq. (13) as a function of z. Red lines are calculated according to Eq. (16).

of $\Phi_9(z)$ the exponential function describing the light wave can be reduced to $\cos(qz)$. The positive and negative values of the product cancel each other in the area shaded in gray, where both approaches give the same z dependence $\Phi_9(z)$. Thus, within this kind of analysis, only the regions lying outside the gray area and neighboring the QW interfaces contribute to the integral (5). Since these are the regions of remarkable difference between the envelopes of the two approaches [see Fig. 5(a) and blue and red areas in Fig. 6(a)], the ratio of radiative decay rates $\Gamma_{0,9}/\Gamma_{0,9}^{\text{c.m.}}$ exceeds a value of 2.5. For the lowest exciton states j, the difference between the functions $\Phi_j(z)$ obtained in the two models is negligible, and the rates Γ_{0j} almost coincide [see the inset in Fig. 6(b)].

Concluding this section, it is necessary to stress that Fig. 6 is a clear illustration of the fact that, for the wide QWs and the high-energy confined states, the interaction of excitons with light is mainly controlled by the interfaces. Moreover, a nonideal character of the interfaces may strongly affect the exciton-light interaction. However, even for ideal interfaces, the interaction may considerably differ from that described by the c.m. model or the polaritonic model, which is described in the next section.

V. EXCITON-LIGHT INTERACTION IN THE POLARITONIC MODEL

The polaritonic model is equivalent to the c.m. model [29] and widely exploited for the description of reflection spectra of heterostructures with very wide QWs [19–23,30]. In the framework of this model, the propagation waves in the well layer are exciton-photon polariton modes satisfying the dispersion relation

$$\varepsilon(\omega, q) = \left(\frac{cq}{\omega}\right)^2, \tag{18}$$

where q is the polariton wave vector. The dielectric function of the constitutive bulk material in the exciton spectral range,

$$\varepsilon(\omega, q) = \varepsilon_b + \epsilon^{hh}(\omega, q) + \epsilon^{lh}(\omega, q), \tag{19}$$

is a sum of the background dielectric constant ε_b and two resonant contributions

$$\epsilon^{\alpha}(\omega, q) = \frac{\omega_{LT}^{\alpha}}{\omega_0 - \omega + \hbar q^2/(2M_\alpha) - i\Gamma_\alpha} \tag{20}$$

from the heavy-hole ($\alpha = hh$) and light-hole ($\alpha = lh$) excitons. Here ω_0 is the bulk exciton resonant frequency, and M_α and Γ_α are the α-exciton translational mass and the nonradiative damping rate. The longitudinal-transverse splittings are related by $\omega_{LT}^{hh} = 3\omega_{LT}^{lh}$. Following [31], we consider the decoupling band scheme of the large-momentum limit which generalizes the c.m. model and allows one to introduce the concept of hh and lh excitons.

The experimentally observed exciton resonances are described in terms of the polariton waves multiply reflected from the internal sides of interfaces, which, for the high-energy spectral range, gives rise to a quasiconfinement of the polariton states [32].

Using the polaritonic model, we have calculated the reflection spectrum of the structure of Fig. 1. The standard Maxwell's boundary conditions together with Pekar's additional boundary conditions (ABCs) are used for the polariton modes at the QW interfaces [33]. The result is shown in Fig. 7.

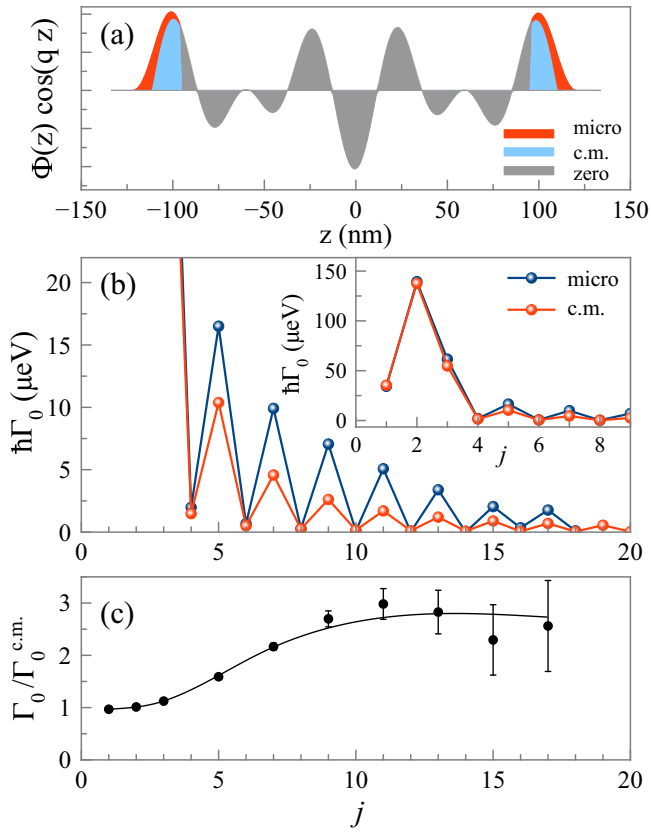

FIG. 6. (a) Product $\Phi_9(z)\cos(qz)$ for the ninth exciton state in the 240-nm GaAs/AlGaAs QW. Gray shading indicates the area which gives no integral contribution to the decay rate $\Gamma_{0,9}$. Light blue areas are the contribution in the c.m. model. Red areas are the additions from the microscopic model. (b) Dependence of $\hbar\Gamma_{0j}$ on the exciton level index j calculated in the microscopic (blue dots) and c.m. (red dots) models. The inset shows the same dependence for small j. (c) Ratio of the radiative damping rates calculated in the microscopic and c.m. models vs the exciton state number j. The errors indicate the inaccuracy of the microscopic calculation, in particular, for $j \geqslant 15$, where the confined exciton states overlap with the unbound electron-hole continuum.

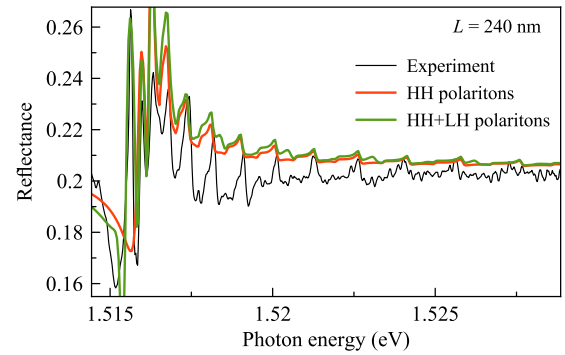

FIG. 7. Comparison of the measured reflection spectrum of the 240-nm QW (black curve) with those calculated in the polaritonic model accounting for only the heavy-hole exciton polariton contribution (red curve) and for both the heavy- and light-hole exciton polaritons (green curve). The model parameters are $\hbar\omega_0 = 1.5158$ eV, $\hbar\omega_{LT}^{hh} = 0.075$ meV, $\hbar\Gamma_{hh} = 0.07$ meV, $\hbar\Gamma_{lh} = 0.12$ meV, $L^\star = 196$ nm.

As seen from Fig. 7, the high-energy resonances in the calculated spectra are less pronounced than in the experimental spectrum. This is an expected result, bearing in mind that the c.m. model underestimates the strength of the interaction of confined excitons with light, as Fig. 6 demonstrated. It is worth mentioning that various forms of the ABCs have been proposed in the literature (e.g., Refs. [16,34–38]). Our results show that, besides the ABCs, correct modeling of the exciton wave functions near the QW interfaces should be included in order to describe the experiment.

VI. CONCLUSION

The experimental study and the theoretical modeling performed in the present work show that the standard model described in Refs. [12–14] is perfectly applicable to the analysis of the high-energy confined exciton states in wide QWs. Its applicability is based on (i) the general analytical properties of the linear resonant response as a function of frequency and (ii) the diminishing role of the light-induced coupling between the confined exciton states with increasing index j. The onset j_0 from which the model is valid for the description of reflectance strongly depends on the QW width. In particular, it can be applied with high accuracy for all the states in a 100-nm QW and with an accuracy of several percent for the states $j \geqslant 6$ in the 300-nm QW. A great advantage of the standard model is, first, its ease of use. Second, it does not require any microscopic modeling of the exciton states and operates with four exciton parameters for each quantum-confined level characterizing the spectral position, intensity, half width, and shape of the corresponding spectral feature. The mixed low-lying confined exciton states with $j < j_0$ should, of course, be described in the framework of the generalized model [15], making allowance for the light-induced coupling between the exciton states. Deep understanding of the exciton-light coupling can be valuable for microcavity polaritons studies [39]. However, reliable tuning of the cavity mode to the excited-state energy to examine exciton-light coupling enhancement experimentally is a challenging problem.

Multiple parameters of the standard model provoke the impression that its better correspondence to experiment stems purely from numerous free parameters. In this paper, the main parameters of the standard model, extracted with fitting, convincingly agree with the parameters obtained from the microscopic calculations (see the inset in Fig. 1). On the contrary, c.m. and polaritonic models contain several free parameters such as transition layer width and averaged hole mass.

We have also compared the exciton-light interaction strength predicted by the c.m. and polaritonic models with that obtained by the numerical solution of the two-particle Schrödinger equation in a rectangular QW. It has been found that both approximate models dramatically underestimate the exciton-light interaction for the excited exciton states. The reason for the underestimation lies in a significant modification of the exciton wave functions near the QW interfaces which cannot be well enough described within the simple models.

ACKNOWLEDGMENTS

Financial support from the Russian Foundation for Basic Research (RFBR, Grant No. 19-52-12059) in the frame of ICRC TRR-160 and from St. Petersburg State University (SPbU, Grant No. 11.34.2.2012 (ID 28874264) and Grant SPbU-DFG 40.65.62.2017 (ID 32806034)) is acknowledged. P.S.G. acknowledges RFBR for the financial support in the frame of Grant No. 18-32-00568. I.V.I. acknowledges RFBR for the financial support in the frame of Grant No. 16-02-00245-a. The authors also thank the SPbU Resource Center "Nanophotonics" for the samples studied in the present work.

[1] L. C. Andreani and A. Pasquarello, Accurate theory of excitons in GaAs − $Ga_{1-x}Al_xAs$ quantum wells, Phys. Rev. B **42**, 8928 (1990).

[2] L. C. Andreani, F. Tassone, and F. Bassani, Radiative lifetime of free excitons in quantum wells, Solid State Commun. **77**, 641 (1991).

[3] B. Deveaud, F. Clerot, N. Roy, K. Satzke, B. Sermage, and D. S. Katzer, Enhanced Radiative Recombination of Free Excitons in GaAs Quantum Wells, Phys. Rev. Lett. **67**, 2355 (1991).

[4] D. S. Citrin, Radiative lifetimes of excitons in quantum wells: Localization and phase-coherence effects, Phys. Rev. B **47**, 3832 (1993).

[5] V. Srinivas, Y. J. Chen, and C. E. C. Wood, Reflectivity of two-dimensional polaritons in GaAs quantum wells, Phys. Rev. B **48**, 12300 (1993).

[6] R. C. Iotti and L. C. Andreani, Crossover from strong to weak confinement for excitons in shallow or narrow quantum wells, Phys. Rev. B **56**, 3922 (1997).

[7] A. D'Andrea, N. Tomassini, L. Ferrari, M. Righini, S. Selci, M. R. Bruni, D. Schiumarini, and M. G. Simeone, Optical properties of stepped $In_xGa_{1-x}As$/GaAs quantum wells, J. Appl. Phys. **83**, 7920 (1998).

[8] A. D. Bristow, T. Zhang, M. E. Siemens, S. T. Cundiff, and R. P. Mirin, Separating homogeneous and inhomogeneous line widths of heavy- and light-hole excitons in weakly disordered semiconductor quantum wells, J. Phys. Chem. B **115**, 5365 (2011).

[9] K. Sivalertporn, L. Mouchliadis, A. L. Ivanov, R. Philp, and E. A. Muljarov, Direct and indirect excitons in semiconductor coupled quantum wells in an applied electric field, Phys. Rev. B **85**, 045207 (2012).

[10] S. V. Poltavtsev, Yu. P. Efimov, Yu. K. Dolgikh, S. A. Eliseev, V. V. Petrov, and V. V. Ovsyankin, Extremely low inhomogeneous broadening of exciton lines in shallow (In, Ga)As/GaAs quantum wells, Solid State Commun. **199**, 47 (2014).

[11] Y. Chen, N. Maharjan, Z. Liu, M. L. Nakarmi, V. V. Chaldyshev, E. V. Kundelev, A. N. Poddubny, A. P. Vasilev, M. A. Yagovkina, and N. M. Shakya, Resonant optical properties of AlGaAs/GaAs multiple-quantum-well based Bragg structure at the second quantum state, J. Appl. Phys. **121**, 103101 (2017).

[12] E. L. Ivchenko, *Optical Spectroscopy of Semiconductor Nanostructures* (Springer, Berlin, 2004).

[13] A. V. Trifonov, S. N. Korotan, A. S. Kurdyubov, I. Ya. Gerlovin, I. V. Ignatiev, Yu. P. Efimov, S. A. Eliseev, V. V. Petrov, Yu. K. Dolgikh, V. V. Ovsyankin, and A. V. Kavokin, Nontrivial relaxation dynamics of excitons in high-quality InGaAs/GaAs quantum wells, Phys. Rev. B **91**, 115307 (2015).

[14] P. S. Grigoryev, A. S. Kurdyubov, M. S. Kuznetsova, I. V. Ignatiev, Yu. P. Efimov, S. A. Eliseev, V. V. Petrov, V. A. Lovtcius, and P. Yu. Shapochkin, Excitons in asymmetric quantum wells, Superlattices Microstruct. **97**, 452 (2016).

[15] M. M. Voronov, E. L. Ivchenko, V. A. Kosobukin, and A. N. Poddubnyi, Specific features in reflectance and absorbance spectra of one-dimensional resonant photonic crystals, Fiz. Tverd. Tela **49**, 1709 (2007) [Phys. Solid State **49**, 1792 (2007)].

[16] H. C. Schneider, F. Jahnke, S. W. Koch, J. Tignon, T. Hasche, and D. S. Chemla, Polariton propagation in high quality semiconductors: Microscopic theory and experiment versus additional boundary conditions, Phys. Rev. B **63**, 045202 (2001).

[17] A. D'Andrea and R. Del Sole, Exciton wave functions in semi-infinite semiconductors: A check of the adiabatic approximation, Phys. Rev. B **32**, 2337 (1985).

[18] D. Schiumarini, N. Tomassini, L. Pilozzi, and A. D'Andrea, Polariton propagation in weak-confinement quantum wells, Phys. Rev. B **82**, 075303 (2010).

[19] A. Tredicucci, Y. Chen, F. Bassani, J. Massies, C. Deparis, and G. Neu, Center-of-mass quantization of excitons and polariton interference in GaAs thin layers, Phys. Rev. B **47**, 10348 (1993).

[20] V. A. Kiselev, B. S. Razbirin, and I. N. Uraltsev, Additional waves and Fabri-Perot interference of photoexcitons (polaritons) in thin II-VI crystals, Phys. Status Solidi B **72**, 161 (1975).

[21] J. J. Davies, D. Wolverson, V. P. Kochereshko, A. V. Platonov, R. T. Cox, J. Cibert, H. Mariette, C. Bodin, C. Gourgon, E. V. Ubylvovk, Y. P. Efimov, and S. A. Eliseev, Motional Enhancement of Exciton Magnetic Moments in Zinc-Blende Semiconductors, Phys. Rev. Lett. **97**, 187403 (2006).

[22] D. K. Loginov, E. V. Ubyivovk, Yu. P. Efimov, V. V. Petrov, S. A. Eliseev, Yu. K. Dolgikh, I. V. Ignatev, V. P. Kochereshko, and A. V. Selkin, Interference of polaritonic waves in structures with wide GaAs/AlGaAs quantum wells, Fiz. Tverd. Tela **48**, 1979 (2006) [Phys. Solid State **48**, 2100 (2006)].

[23] D. K. Loginov, A. V. Trifonov, and I. V. Ignatiev, Effect of uniaxial stress on the interference of polaritonic waves in wide quantum wells, Phys. Rev. B **90**, 075306 (2014).

[24] S. Yu. Bodnar, P. S. Grigoryev, D. K. Loginov, V. G. Davydov, Yu. P. Efimov, S. A. Eliseev, V. A. Lovtcius, E. V. Ubyivovk, V. Yu. Mikhailovskii, and I. V. Ignatiev, Exciton mass increase in a GaAs/AlGaAs quantum well in a transverse magnetic field, Phys. Rev. B **95**, 195311 (2017).

[25] E. L. Ivchenko, V. P. Kochereshko, A. V. Platonov, D. R. Yakovlev, A. Wang, B. Ossau, and G. Landwehr, Resonant optical spectroscopy of long-period quantum-well structures, Fiz. Tverd. Tela **39**, 2072 (1997) [Phys. Solid State **39**, 1852 (1997)].

[26] E. S. Khramtsov, P. A. Belov, P. S. Grigoryev, I. V. Ignatiev, S. Yu. Verbin, Yu. P. Efimov, S. A. Eliseev, V. A. Lovtcius, V. V. Petrov, and S. L. Yakovlev, Radiative decay rate of excitons in square quantum wells: Microscopic modeling and experiment, J. Appl. Phys. **119**, 184301 (2016).

[27] P. S. Grigoryev, O. A. Yugov, S. A. Eliseev, Yu. P. Efimov, V. A. Lovtcius, V. V. Petrov, V. F. Sapega, and I. V. Ignatiev, Inversion

of Zeeman splitting of exciton states in InGaAs quantum wells, Phys. Rev. B **93**, 205425 (2016).

[28] A. V. Trifonov, Y. P. Efimov, S. A. Eliseev, V. A. Lovtcius, P. Y. Shapochkin, and I. V. Ignatiev, Dynamics of excitonic polaritons in semiconductor heterostructures with quantum wells, in *2017 Progress In Electromagnetics Research Symposium - Spring (PIERS)* (IEEE, Piscataway, NJ, 2017), p. 2566.

[29] V. A. Kiselev, I. V. Makarenko, B. S. Razbirin, and I. N. Uraltsev, Size quantizing of excitons, Fiz. Tverd. Tela **19**, 1348 (1975) [Sov. Phys. Solid State **19**, 1374 (1975)].

[30] E. Ubyivovk, Yu. K. Dolgikh, Yu. P. Efimov, S. A. Eliseev, I. Ya. Gerlovin, I. V. Ignatiev, V. V. Petrov, and V. V. Ovsyankin, Spectroscopy of high-energy excitonic states in ultra-thick GaAs quantum wells with a perfect crystal structure, J. Lumin. **102–103**, 751 (2003).

[31] E. O. Kane, Exciton dispersion in degenerate bands, Phys. Rev. B **11**, 3850 (1975).

[32] V. A. Kiselev, I. N. Uraltsev, and I. V. Makarenko, Size effects on polaritons in thin crystals with perfect interference spectra, Solid State Commun. **53**, 591 (1985).

[33] S. I. Pekar, The Theory of Electromagnetic Waves in a Crystal in which Excitons are Produced, Zh. Eksp. Teor. Fiz. **33**, 1022 (1957) [Sov. Phys. JETP **6**, 785 (1958)].

[34] *Excitons*, edited by E. I. Rashba and M. D. Sturge (North-Holland, Amsterdam, 1982).

[35] G. Makov and M. C. Payne, Periodic boundary conditions in *ab initio* calculations, Phys. Rev. B **51**, 4014 (1995).

[36] K. Henneberger, Additional Boundary Conditions: An Historical Mistake, Phys. Rev. Lett. **80**, 2889 (1998).

[37] E. A. Muljarov and R. Zimmermann, Exciton polariton including continuum states: Microscopic versus additional boundary conditions, Phys. Rev. B **66**, 235319 (2002).

[38] S. I. Maslovski, T. A. Morgado, M. G. Silveirinha, C. S. R. Kaipa, and A. B. Yakovlev, Generalized additional boundary conditions for wire media, New J. Phys. **12**, 113047 (2010).

[39] A. V. Kavokin, J. J. Baumberg, G. Malpuech, and F. P. Laussy, *Microcavities*, 2nd ed. (Oxford University Press, Oxford, 2017).